AD-A064 857 MISSOURI UNIV-ROLLA F/G 17/5
CLOUD CHAMBER INFRARED MEASUREMENTS.(U)
JAN 78 D R WHITE DAAK70-76-C-0246
UNCLASSIFIED NL

| OF |
AD
A064857

END
DATE
FILMED
4-79
DDC

# CLOUD CHAMBER INFRARED MEASUREMENTS

Final Report

Contract No. DAAK70-76-C-0246

January, 1978

by

Daniel R. White

prepared for

Department of the Army
U.S. Army Mobility Equipment Research and Development Command
Night Vision Laboratory
Ft. Belvoir, Virgina 22060

## ABSTRACT

During the report period, ~~of this contract~~ the design of the simulation chamber ~~has been~~ was established, initial thermal tests ~~have been~~ were conducted, and a study of the procedure for making the desired IR attenuation and scattering measurements ~~has been~~ was made. Limitations of both time and funds have not permitted the project to be carried through to the point of making actual IR measurements.

The project is being continued subject to available funding from a variety of sources.

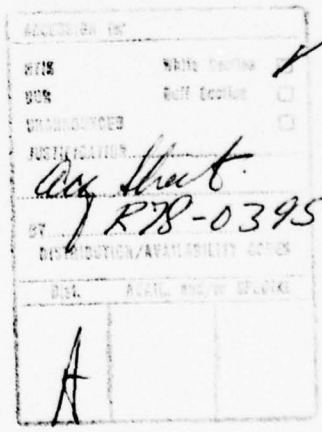

# I. Introduction

The overall program of work planned for this project includes:

1) Design of a full size cloud simulation chamber,
2) Construction and performance testing of a single section of the chamber, and
3) Attempt to make scattering and attenuation measurements of infrared radiation in clouds and fogs.

Success has varied widely between the three items. Item 1 has been the most successful with completion of the design of the major chamber parts; however, numerous details associated with support hardware are yet to be decided. Item 2 has been limited to work with a small test section representing one-twenty fourth of a chamber side wall section. Work on Item 3 has consisted of some feasibility studies and planning for procedures required.

# II. Description of work

## A. Design of full size cloud simulation chamber

The current design of the full size cloud simulation chamber is given in the accompanying set of machine shop drawings. The basic approach has been changed from a two phase refrigeration cooling system for temperature control of the interior wall surface to a thermoelectric cooled inner wall. The thermoelectric design has always been the preferred technique based on versatility, compute compatibility, speed of response, quality and ease of control. However, at the time the proposal was submitted, calculations of interior surface temperature uniformity as a function of inner wall thickness predicted the need for a 2.54 cm. thick inner wall to meet required uniformity tolerances, this resulted in an effective heat capacity per thermoelectric module which made it impossible to meet the required maximum cooling rate of 15°c/min. We have since circumvented the problem by using a laminated aluminum inner wall having an anisotropic thermal conductivity.

This combines the smoothing properties of the thick plate with the smaller heat capacity of a thin plate.

The initial design was then developed based on previous computer heat transfer studies, experience gained from work with the present prototype chamber, and mechanical and fabrication restrictions. A pictorial drawing of the complete chamber is shown in Fig. 1. The chamber consists of flat top and bottom plate assemblies and seven cylindrical side wall assemblies which can be stacked in any sequence. This permits modifications made to one section to be used at any level of the chamber.

Fig. 2 shows a cross section of a side wall. The inner wall plate is formed by bonding a 6.35mm aluminum plate and a 3.17mm aluminum plate together with "Melt Bond 1133" (Narmco Materials, Inc., Costa Mesa, CA). The outer 5.72cm aluminum wall serves as a heat sink for the thermoelectric modules, therefore heat transfer from the heat sink to the inner wall past the thermoelectrics must be minimized. The studs extending from the inner wall plate out through the heat sink provide the compression necessary for proper heat transfer to and from the thermoelectric modules. The O-ring seal around the perimeter of the inner wall plate together with those around the expansion parts form part of the primary chamber sensitive volume seal. The seals around the studs and inner wall thermometer serve as a secondary seal to permit maintainence of a vacuum around the thermoelectric modules. This reduces the reverse heat flow from the heat sink to the inner wall.

The temperature of the heat sink is maintained by a flow of thermally regulated liquid through passages located near the outer surface. The passages are interconnected in pairs so that liquid which flows down one passage returns through the adjacent passage, both passages are behind a single row of thermoelectric modules. The double-back flow pattern compensates for the increase in liquid temperature as it passes through the heat sink. The resulting

heat sink temperature as seen by the thermoelectric modules is the average of the inlet and outlet temperatures. Flow paths are verticle in the side walls and parallel to the long dimension of the inner wall plates on the top and bottom. The external manifolding, only a portion of which is shown in Fig. 1, is designed so that a given volume of liquid makes only a single pass through the heat sink before being returned to the main reservoir. Each of the nine major chamber assemblies forms an independent flow path between the main inlet and return lines, this insures adequate flow in all units regardless of the number in use. It is estimated that a flow of 1.4 l/sec per section will be required at maximum cooling.

The expansion of the sensitive volume is accomplished by drawing air out through numerous small ports evenly distributed over the chamber side walls. Each interior side wall plate contains thirty-six parts. The external manifolding has been designed to produce equal air flow through all ports. This results in an expansion of the sensitive volume in which air motion is confined to the horizontal plane with radial symmetry about the central axis of the chamber. Any vertical air motion caused by the discrete nature of the ports is localized in the vicinity of the walls with an average of zero. The flow calculations used to determine passage sizes in the external manifolds are given in Appendix A.

The expansion manifold will also be used for sample introduction. All the individual manifold layers, only a portion of which are shown in Fig. 1, are connected by four vertical mains spaced at 90° intervals around the chamber. If these mains are clocked just above the bottom side wall assembly and just below the top side wall assembly any air flow entering the system at the bottom and being exhausted at the top will have to pass through the sensitive volume. This technique eliminates the mechanical complexity and thermal anomally of separate sample inlet

and outlet ports. Theoretical calculations of the effects on aerosol size distribution caused by passage through the inlet manifold are given in Appendix B.

B. Construction and Thermal Tests

Once the basic design of the heat sink and inner wall was decided, a small test section was constructed. This unit represents half of one of the twelve faces of a side wall assemb16. This also represents the interior surfaces which are cooled by a single controller-power supply unit. The test section has twenty thermoelectric modules (Barg Warner Thermoelectric - Model 940-31) mounted in a 4 by 5 rectangular array. In the full size chamber, each of the twelve faces of a side wall assembly will have fourty thermoelectric modules in a 4 x 10 array with each of the two 4 x 5 halves having its own controller-power supply.

The controller-power supplies developed for the current prototype chamber do not have either the voltage or current capability to provide full power to twenty thermoelectric modules (14 amps @ 70 VDC). This forced us to use manual control for all tests with the power supply in either the constant current or constant voltage mode.

The first test was a measure of the maximum cooling rate to insure that the required 15°c/min could be achieved. The results showed that for as much as 10°c below the heat sink temperature, the inner wall could be cooled at rates in excess of 15°c/min. Rates as high as 25°c/min were measured for wall temperatures very near the heat sink temperature. These results should be taken as a minimum performance test since they were conducted without a vacuum between the inner wall and heat sink, and we were still searching for the optimum thermal contact between the thermoelectrics and adjacent surfaces. The measurements were made using one of the transistor thermometers developed in this laboratory (See Appendix C) mounted in a smooth hole boxed in the inner wall plate. The sensor response time may have lowered the maximum measured cooling rate.

The sensor mount has since been redesigned and the response time reduced from approximately 7 seconds to approximately 4 seconds.

The next tests were to measure the uniformity of surface temperature of the inner wall plate as a function of thermoelectric current. Plans to photograph the location of hot or cold spots depicted by a sheet of liquid crystal paper attached to the front of the inner plate failed due to difficulty in achieving a uniform contact between paper and plate and effects of the ambient temperature on the uninsulated surface. Thin film thermocouples were attached to the surface of the inner wall plate representing the interior chamber wall in the configuration shown in Fig. 3. The dotted squares show the location of the thermoelectric modules, the x's are the thermocouple locations and the circle is the transistor thermometer. The test section was insulated with three layers of polyethylene foam 1.27 cm thick laminated with two layers of aluminum foil. The foam has a thermal conductivity of 0.036 W/MK. The heat sink coolant was water circulated through a closed loop system containing a refrigerated heat exchanger for removal of the excess heat. The test section was supported in an upright position to duplicate the orientation in the final assembly and to insure that the coolant passages remained filled with water.

During the tests, the power supply for the thermoelectrics was adjusted to provide the desired current, then the system was allowed to cone to a steady state condition. At this point the temperature difference between the two surface points being tested was recorded. The results for the three measured differences are shown in Fig. 4 for currents up to 7 amps. The difference $\Delta T_{2_3}$ is in the expected direction and while slightly larger than desired, is small enough to work with since it represents a short range ripple which will be smoothed out only a short distance from the wall.

While not tested at this time, it is felt that the major contribution to the differences $\Delta T_{21}$ and $\Delta T_{24}$ was caused by the need to parallel the wiring of horizontal rows of thermoelectric modules. This was due to voltage limits of the power supplies available. Our previous experience with parallel wiring has shown that this can happen due to slight differences in the electrical resistance of different modules. It should be noted that the difference $\Delta T_{14} = \Delta T_{24} - \Delta T_{21}$ remains small. Other possible sources requiring further investigation are variations in heat sink temperature, convection of the air surrounding the thermoelectric modules, and variations in thermoelectric compression force. Further tests at higher currents and with all units in series are also required.

C. Infrared Scattering and Attenuation

The transparency of the atmosphere which makes infrared radiation so useful for detection, surveillance, electrooptical control and guidance applications is the same feature which makes laboratory measurements of attenuation so difficult. Typical attenuation measurements are made using optical paths of kilometer length to provide sufficient attenuation to achieve an adequate signal to noise ratio. However, this makes it impossible to measure the atmospheric parameters along the entire path with the desired accuracy if a straight line path is used. The cloud simulation chamber being designed can provide the required knowledge of the atmospheric parameters but puts severe restrictions on the physical size of the system.

By utilizing windows located in the top and bottom of the chamber, a physical path length of 2.85m can be obtained. The proposed window design (see machine drawings) is compatible with use in both the top and bottom plates as well as the side walls. The design also permits the addition of extra windows with relatively simple modifications.

Some preliminary tests using a low power CW laser

operating in the visible red have led to the conclusion that it is feasible to utilize a white cell to obtain a large number of reflections of the beam between two spherical mirrors. This would permit the optical path length to be increased to the required lengths while remaining within the physical constrains of the chamber. The tests also indicated that the system should be relatively easy to align. Small change in alignment occuring during uses should not greatly effect operation.

In the case of scattering, measurements will be made using a horizontal beam through the chamber. The initial side wall design places windows at relative angles of 0°, 30°, 90°, 180°, 210°, and 270° around the chamber; however, if necessary additional windows at any multiple of 30° can be added with relative ease. It is not expected that the scattering measurements will require a multipass optical path but this would not cause any major problem if necessary.

An examination of the present technology of IR sources and detectors appears to indicate the use of one of two basic choices. In one case, the source would consist of a standard and relatively inexpensive black body or globar which are physically large and produce a low intensity. These sources would require at least a liquid nitrogen cooled detector (mercury cadmium telluride) resulting in an expensive sophisticated system requiring constant maintainance. The other case would use a relatively inexpensive pyroelectric detector (lithuim tantalate or polyvinylidene fluoride) but would need one of the high intensity laser diodes or IR tunable lasers, both of which are still relatively new and expensive. The present lasers also require constant attention from a highly qualified research staff member.

While the statements above seem to give little help in choosing between the two systems, we are currently planning on using the pyroelectric detector and either

laser or laser diode source for two reasons. First, as the development of both the IR tunable laser and laser diodes progresses, they will undoubtedly become more reliable, easier to maintain, and less expensive. There appears to be little reason to expect any significant changes in their areas with the liquid nitrogen cooled detectors. Second, by using an existing $CO_2$ laser at 10 microns, the system can be designed, tested, and initial data at 10 microns collected prior to the expendure of funds for the most expensive part of the system.

The use of the existing $CO_2$ laser would also permit the development of the optics to be pushed ahead separate from the chamber construction thereby permitting early solution to such problems as aerosol collection on mirrors and windows. The completed system would then be transferred to the chamber when required.

## III. Summary and Future Work

During the period covered by this contract, we have completed the design of the major chamber components, performed the initial thermal tests of the design, made a comparative survey to determine the best choice of optical system, and made preliminary tests to further verify the feasibility of making IR attenuation measurements in the chamber. Limitations of both time and funds have prevented us from progressing beyond these early stages to the point of making actual measurements of either IR scattering or attenuation at this time. Based on the work completed to date, we are confident that the cloud simulation chamber being developed here can provide the type and quality of atmospheric radiation measurements required to support the work of the Night Vision Laboratory.

It is our current plan to continue with the development and construction of the chamber described in this report. Due to the versatility of the chamber, funds are being sought from a number of federal agencies and several private corpora-

tions which have interests in areas of atmospheric research which could benefit from work with this chamber. We also feel that the size of the total project which has a current estimated budget of $1.25 million dollars over a four year period would be beyond the resources of any one agency interested in this area of research. In developing the present budget and schedule estimates we have tried to be as realistic and complete as possible at this time.

At the present time pending additional funding, we are continuing the project using whatever funds and manpower can be spared from our other projects.

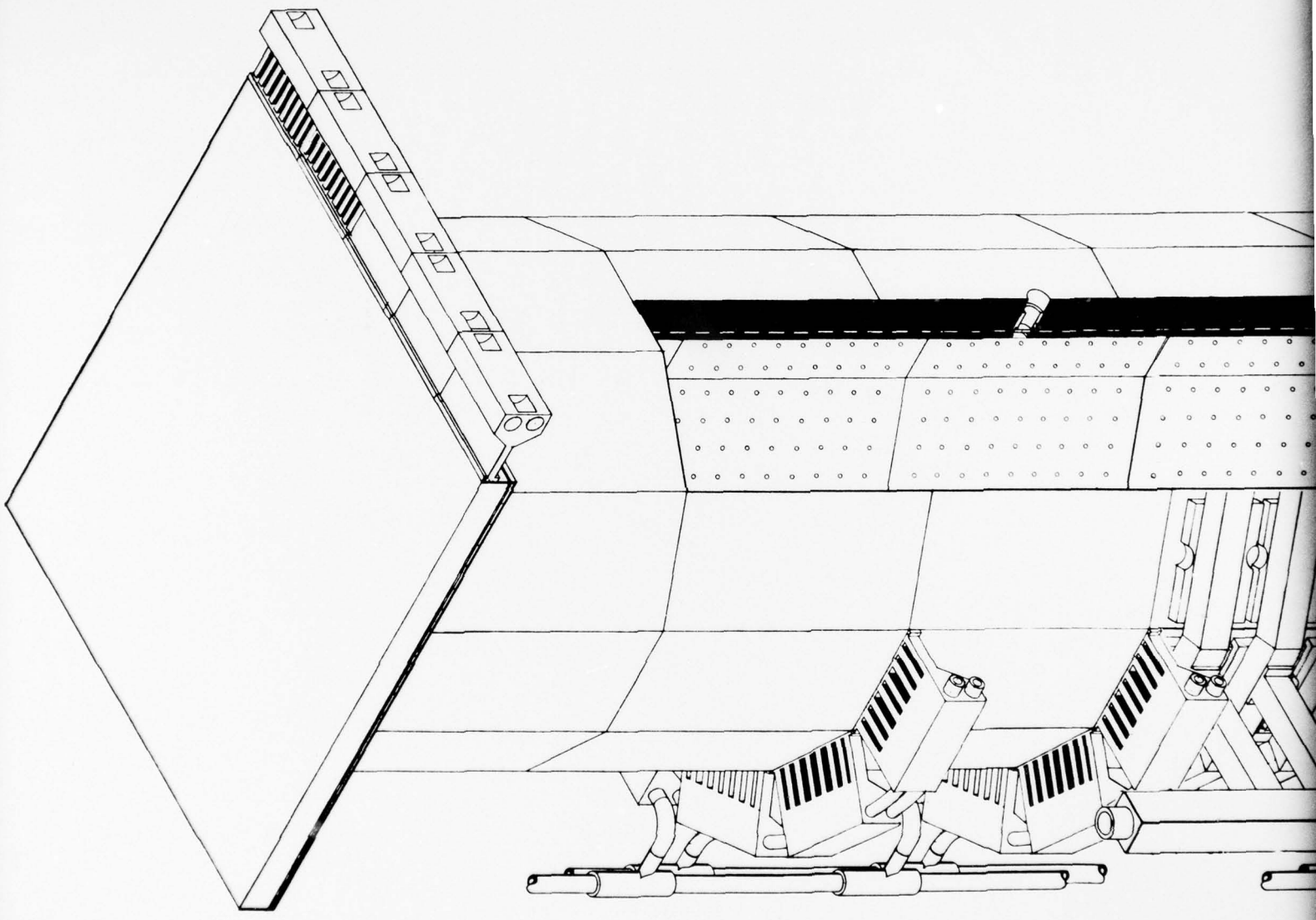

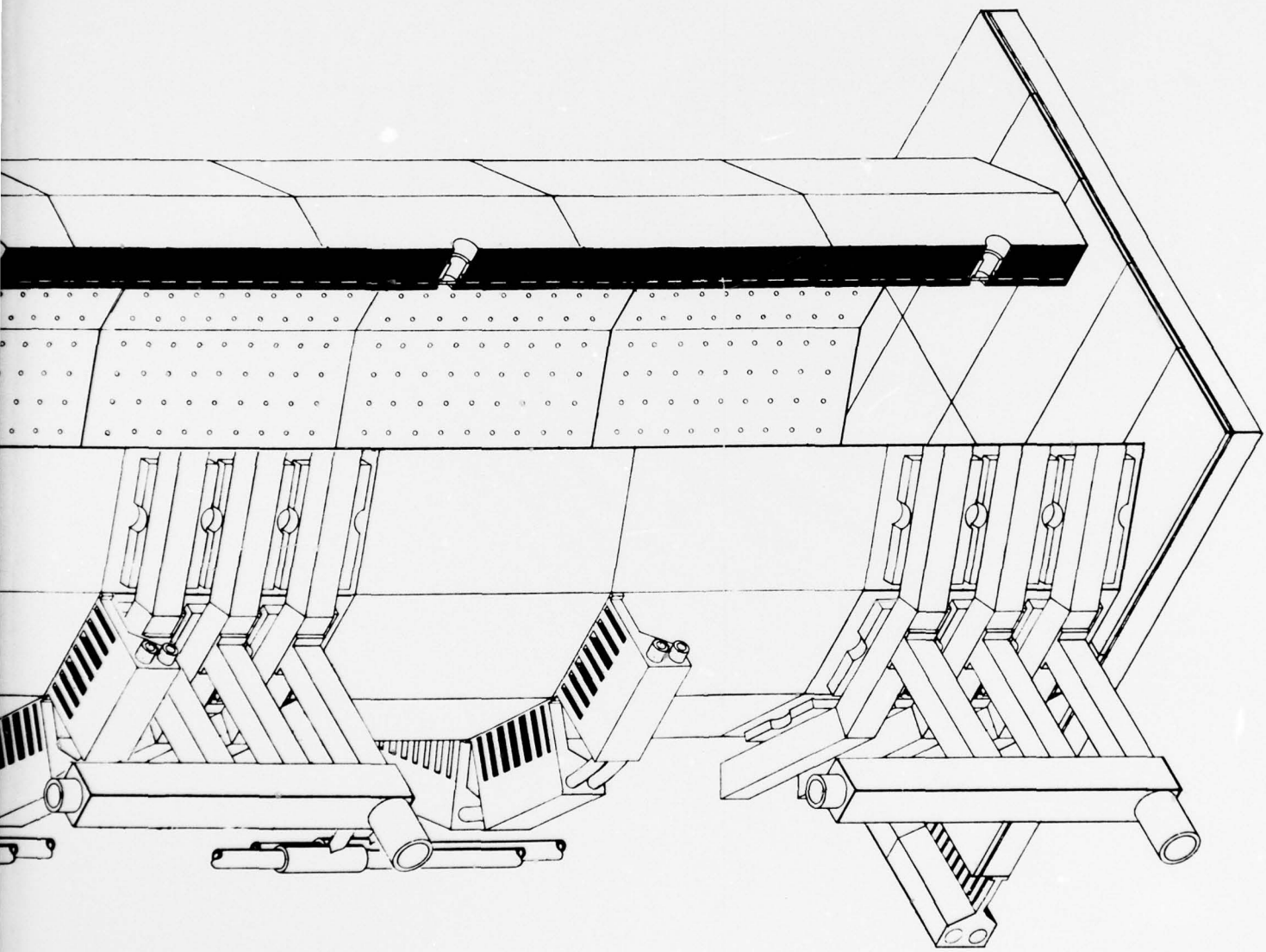

Fig. 1 Cloud Simulation Chamber

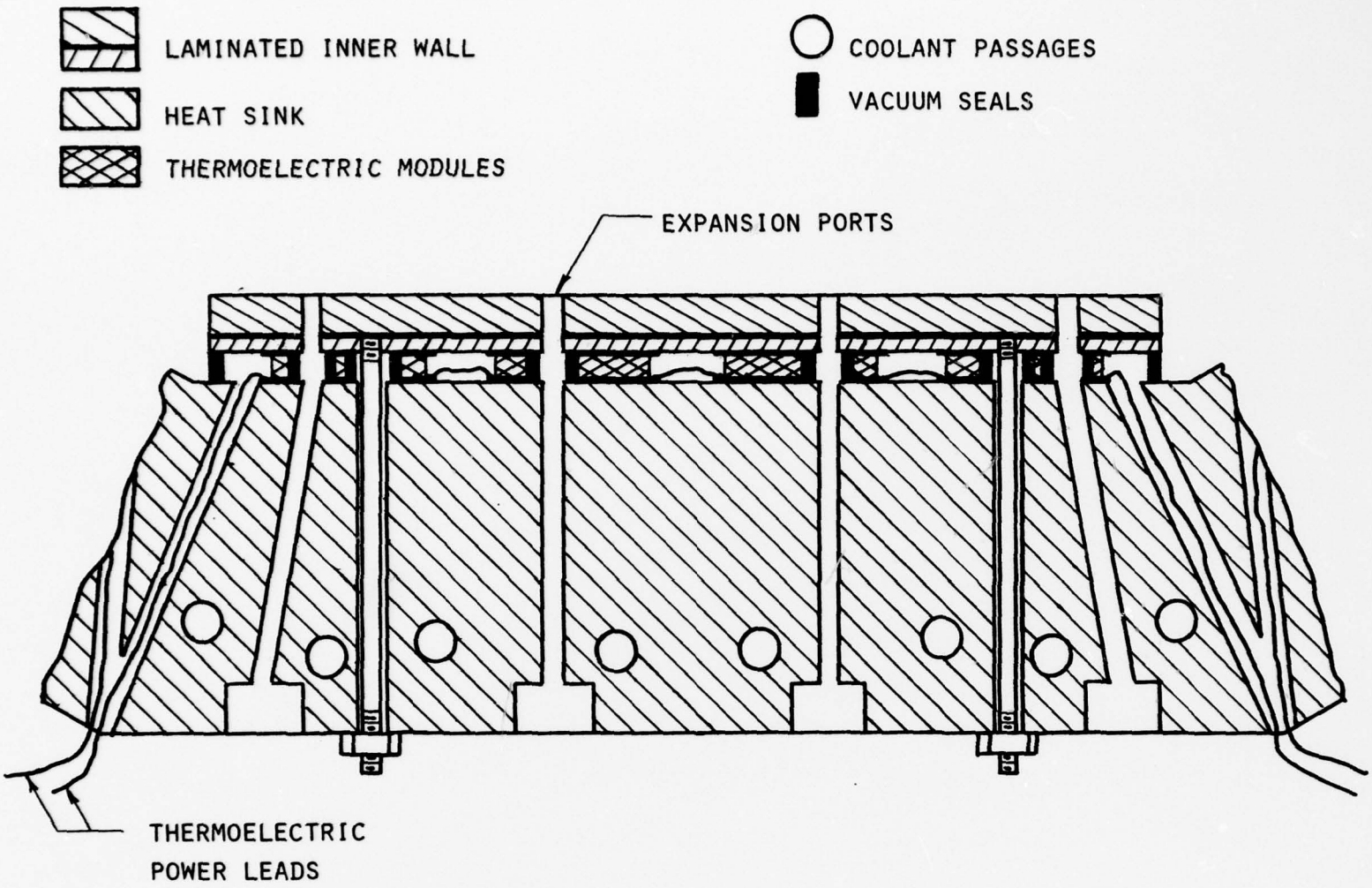


FIG 2. CROSS-SECTION OF CHAMBER WALL

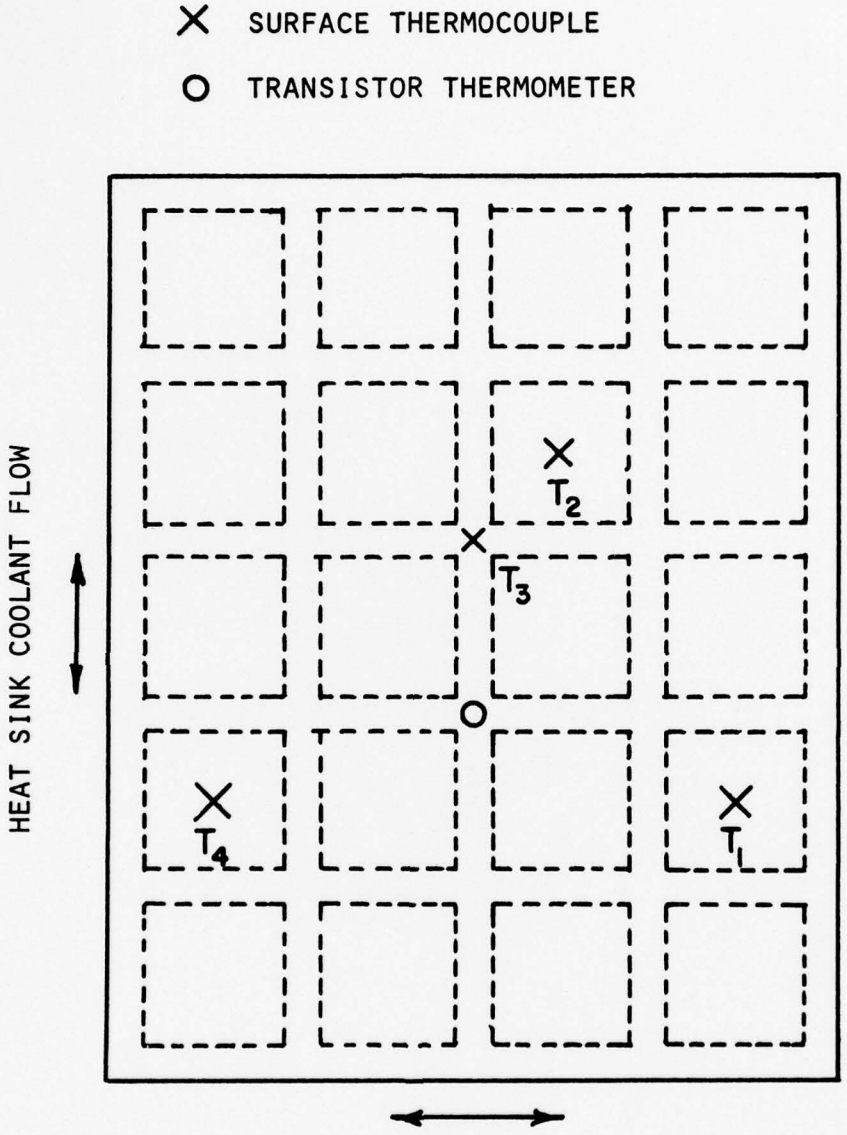


FIG 3. LOCATION OF TEMPERATURE SENSORS DURING THERMAL TESTS

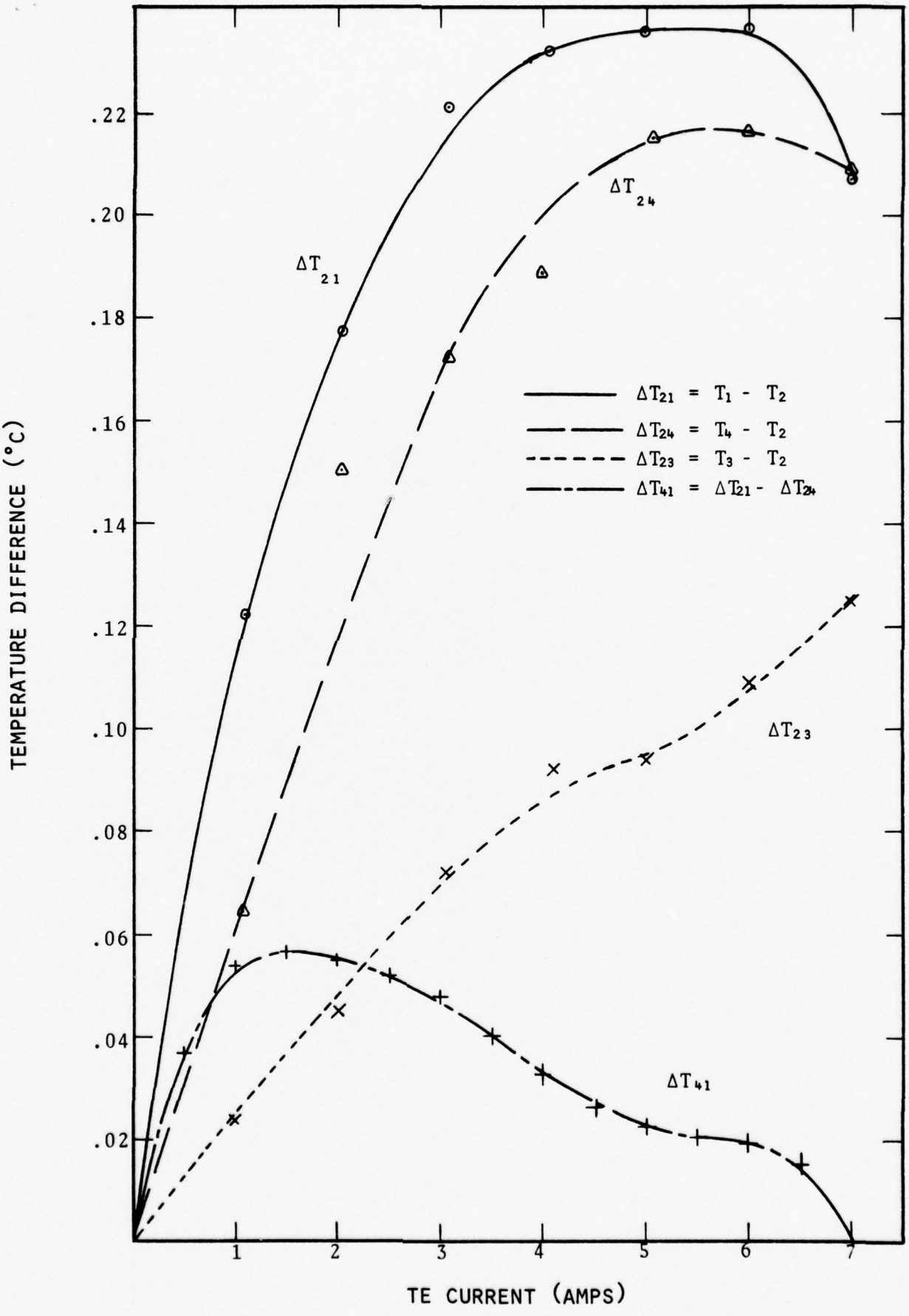


FIG 4. INNER WALL SURFACE TEMPERATURE DIFFERENCES VS THERMOELECTRIC CURRENT

# NEW SIMULATION CHAMBER-ROMULUS ANALYSIS OF EXPANSION MANIFOLD FLOW (1-8)

D. J. Schleuter - D. R. White

## I. Introduction

The purpose of this study is to adjust the design of the expansion manifold to insure uniform volumetric flow from all interior parts. Removal from the manifold system will be at four equal spaced points around the chamber. Calculation will be based on the flow requirements of a dry adiabatic expansion of $15^{o}C/min$ at room temperature and atmospheric pressure.

Interior expansion parts from a grid four parts wide and nine parts high on each of the twelve side of the chamber side wall section. Each minifold covers a grid four parts wide and three high, so there are three manifolds required to cover each section. The twelve manifolds surrounding the chamber at a given level are all interconnected to increase pressure uniformity.

## II. Calculations

A. Volumetric change per second associated with each manifold.

Chamber volume per manifold is a triangular prism

$V_o = 1/2\ abh \qquad a=12in\ ,\ b=6.425in\ ,\ h=5.33in$

$V_o = 205.47in^3$

$$V_2 = V_1 \left( {}^{T_1}/_{T_2} \right)^{\frac{1}{\gamma - 1}}$$

$$V_2 - V_1 = V_1 \left[ (T_1/T_2)^{\frac{1}{\gamma - 1}} - 1 \right]$$

$T_1 = 20^{o}C = 293.16^{o}K \qquad T_2 = 19.75^{o}C = 292.91^{o}K$

$\gamma = 1.4$ adiabatic index for air

$V_1=V_o=205.47 in^3$

$\Delta V_m = V_2-V_1 = .439\ in^3/sec$ per expansion manifold

$\Delta V_p = {}^{\Delta Vm}/_{12} = .036\ in^3/sec$ per interior port

B. Density of the air

$\nu_1 = {}^{RT_1}/_{P_1}$ $\qquad R=53.34\ \frac{ft-\#}{\#\ {}^oR}$

$T_1 = 528\ {}^oR$

$P_1 = 14.0\ \#/in^2$

$\nu_1 = 13.97\ ft^3/\#$

$\nu_2 = \nu_1(\frac{528}{527.55})^{2.5} = 14.00\ ft^3/\#$

$\nu_{avg} = 1/2(\nu_2+\nu_1) = 13.98\ ft^3/\#$

$\rho = {}^1/_{\nu\ avg} = .0715\ \#/ft^3 = 4.138x10^{-8}\ \#/in^3$

C. Passages from interior surface to manifold entrance two passage configuartion shown in Fig. 1

Fig. 1a represents the two center columns of ports on a side while Fig. 1b represents the two outside columns.

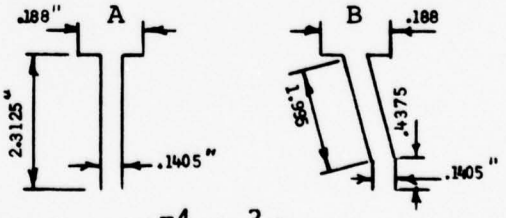


Fig 1

Kenematic viscosity of air $\nu=1.-x10^{-4}\ ft^2/sec$

air velocity in passage 1a

$$\nu_1 = \frac{\Delta V_p}{A} = \frac{.036}{\frac{\pi}{4}(.1405)^2} = 2.32\ in/sec$$

$$Re = {}_1d/\nu = (2.32)(.1405)/(1.6x10^{-4})(144) = 14.15$$

$f = 64/Re = 4.52$

passage length $L=2.3125$ in

less factor (K)

entrance $K=.34$

exit $K=(1-d_1^2/d_2^2)^2 = .20$

Total $K= .54$

$$\Delta p = \frac{\rho f L v_1^2}{2dg} + \rho\frac{K v_1^2}{2g} \qquad g= 32.2 \text{ ft/sec}^2$$

$$= \rho\frac{v1^2}{2g}\left[\frac{fL}{d} + K\right] = 2.16 \times 10^{-5} \#/in^2$$

The effective length of passage 16 is increased by 8 diameters due to the bend

$$\Delta p = \frac{\rho v^2}{2g}\left[\frac{fL^e}{d} + K\right] = 2.16 \times 10^{-5} \#/in^2$$

$p = 4.138\#1/in^3$

$g = 32.2 \text{ ft/sec}^2$

$$f = \frac{64}{Re} = \frac{64\nu}{\nu\alpha} =$$

$\nu = 1.6 \times 10^{-4} ft^2/sec$

$$v = \frac{4\Delta Vp}{\pi\alpha^2}$$

$\Delta V_p = .036 \text{ in}^3/\text{sec}$

$L_e = 2.4325 + 8\alpha$

$K = .54$

Substitute and solve forth order equation for d by iteration

$d = .1579$ in.

Therefore use #21 drill $d = .159$ in

D. Passages from entrance to manifold to horizontal collection passage (Fig. 2)

Hole Diameters (Trial Sizes)

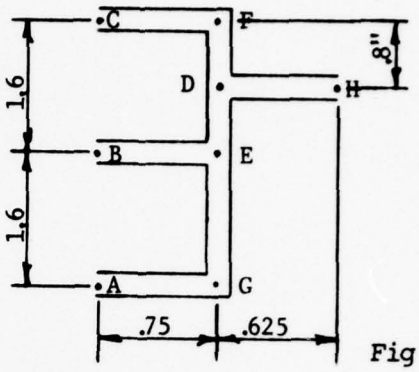

Fig 2

AG=BE=CF=DH=.188in

FD = .156in

GD = .222in

$$\Delta p(CF)=\Delta p(BE)=\Delta p(AG)= \frac{\rho f L v^2}{2gd}$$

$\rho = 4.138 \times 10^{-5} \#/in^3$ $\quad g = 386.4\ in/sec^2$

d = .188in $\quad L = .75 + 50d = 10.15 \quad \nu = 2.304 \times 10^{-2} in^2/sec$

$$\Delta V_p = .036 in^3/sec \quad v = \frac{4\Delta V_Q}{\pi\alpha^2} = 1.297 in/sec$$

$$f = \frac{64}{R_e} = \frac{64\nu}{v\alpha} = 6.047$$

$$\Delta p = 2.94 \times 10^{-5}\ \#/in^2$$

$\Delta p(FD)$

d=.156in $\quad$ L=.8+50d=B.6in

v=1.883in/sec $\quad$ f=5.02

$\Delta p(FD)=5.253 \times 10^{-5} \#/in^2$

$\Delta p(CD)=8.2 \times 10^{-5} \#/in^2$

$$\Delta p(BE)=\Delta p(AE) = \frac{\rho f_{BE} L_{BE} v_{BE}^2}{2d_{BE}g} = \frac{\rho f_{AG} L_{AG} v_{AG}^2}{2d_{AG}g} + \frac{\rho f_{GE} L_{GE} v_{GE}^2}{2d_{GE}g}$$

$$f_{BE} = \frac{16\nu\pi d_{BE}}{Q_B} \qquad f_{AG} = \frac{16\nu\pi d_{AG}}{Q_A} \qquad f_{GE} = \frac{16\nu\pi d_{GE}}{Q_A}$$

$L_{BE}= (.75+50d_{BE})$ $L_{AG}= (.75+50d_{AG})$ $L_{GE}= (1.6+20d_{GE})$

$$v_{BE}= \frac{4Q_B}{\pi d_{BE}^2} \qquad v_{AG}= \frac{4Q_A}{\pi d_{AG}^2} \qquad v_{GE}= \frac{4Q_A}{\pi d_{GE}^2}$$

Substituting $$\frac{L_{BE}\,Q_B}{d_{BE}^4} = \frac{L_{AG}Q_A}{d_{BE}^4} + \frac{L_{GE}Q_A}{d_{BE}^4}$$

$$(.75+50d_{BE})d_{BE}^{-4}Q_B=\{(.75+50d_{AG})d_{AG}^{-4}+(1.6+20d_{GE}^{-4}\}Q_A$$

Requrie $Q_A=Q_B$ $d_{BE}=.188in$ $d_{GE}=.222in$

then $d_{AG}=.212in$ use #3 drill $d_{AG}=.213in$

$$\Delta p(BE)= {}^{\rho f_{BE}L_{BE}v_{BE}^2}/_{2d_{BE}g}$$

$$= 2.94 \times 10^5 \#/in^2$$

$$\Delta p(FD) = \Delta p(ED) = \frac{\rho f_{FD}L_{FD}v_{FD}^2}{2gd_{FD}} = \frac{\rho f_{ED}L_{ED}v_{ED}^2}{2gd_{ED}}$$

$$\frac{L_{FD}Q_C}{d_{FD}^4} = \frac{L_{ED}(Q_A+Q_B)}{d_{ED}^4}$$

$L_{FD}= (.8+50d_{FD})$ $L_{ED}= (.8+50d_{ED})$

$2Q_C= Q_A + Q_B$

$$(.8+50d_{FD})d_{FD}^{-4} = 2(.8+50d_{ED})d_{ED}^{-4}$$

$d_{ED}=.222in$

$d_{FD}=.177in$ #16 drill $\Delta p(FD)=3.756 \times 10^{-5} \#/in^2$

E. Horizontal collection passage (Fig. 3)

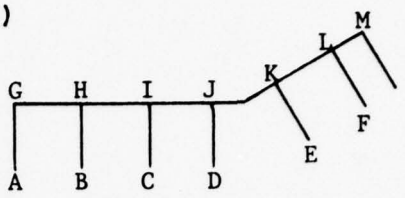

Fig 3

lengths AG,BH,CI,DJ,EK,FL=0.625in

GH = IJ = KL = 1.903 in; LM=.872 in

JK = 2.987 in; HI= 1.744 in

Assume diameters AG,BH,CI,DJ,EK & FL = 0.188 in

Assume diameter of horizontal collection passage = 1.250 in

Determine distribution of flow

$$\Delta P_{AG} = \frac{\rho f_{AG} L_{AG} v_{AG}^2}{2gd_{AG}} + \frac{\rho k v_{AG}^2}{2g} = 1.90 \times 10^{-6} \#/in^2$$

$Q = 3(.036) in^3/sec$

$L_{AG} = .625$ K=1 $d_{AG} = .188$ in

$\Delta P_G = [2.16 + 2.94 + 3.756 + .190] \times 10^{-5} = 9.046 \times 10^{-5} \#/in^2$

pressure drop from inside of chamber to horizontal collection passage for $Q = .036\ in^3/sec$

$$\Delta P_{GH} = \frac{\rho f_{GH} L_{GH} v_{GH}^2}{2gd_{GH}} = 8.463 \times 10^{-9} \#/in^2$$

$L_{GH} = 1.903$ in $d_{GH} = 1.250$ in $Q = 3(.036) in^3/sec$

$$\Delta P_{HI} = \frac{\rho f_{HI} L_{HI} v_{HI}^2}{2gd_{HI}} = 1.55 \times 10^{-8} \#/in^2$$

$L_{HI} = 1.744$ in d#J = 1.250 $Q = 6(.036)\ in^3/sec$

$\Delta P_I = 9.048 \times 10^{-5} \#/in^2$

$Q_{AG}/Q_{CI} = \Delta p_G/\Delta p_I = .9997$

$$\Delta P_{IJ} = \frac{\rho f_{Ij} L_{Ij} v_{Ij}^2}{2g d_{IJ}} = 2.538 \times 10^{-8} \#/in^2$$

$L_{IJ} = 1.903$ in $\quad d_{IJ} = 1.250 \quad Q = 9(.036)$ in$^3$/sec

$$\Delta P_J = 9.050 \times 10^{-5} \#/in^2$$

$$Q_{AG}/Q_{DJ} = \Delta P_G/\Delta P_J = .9995$$

$$\Delta P_{jk} = \frac{\rho f_{jk} L_{jk} v_{jk}^2}{2g d_{jk}} = 2.310 \times 10^{-7} \#/in^2$$

$L_{JK} = 2.987 + 8(1.25) \quad d_{jk} = 1.25 \quad Q = 12(.036)$ in$^3$/sec

$= 12.987$

$$\Delta P_K = 9.073 \times 10^{-5} \#/in^2$$

$$Q_{AG}/Q_{EK} = \Delta P_G/\Delta P_K = .9970$$

$$\Delta P_{KL} = \frac{\rho f_{KL} L_{KL} v_{KL}^2}{2g d_{KL}} = 4.233 \times 10^{-8} \#/in^2$$

$L_{KL} = 1.903$ in $\quad d_{KL} = 1.250$ in $\quad Q = 15(.036)$ in$^3$/sec

$$\Delta P_L = 9.077 \times 10^{-5} \#/in^2$$

$$Q_{AG}/Q_{FL} = \Delta P_G/\Delta P_L = .9966$$

$$Q_{FL} = 1.003\ Q_{AG}$$

which considering the accuracy of the calculatious is no significant change.

Remaining lines will be sized to keep differences insignificant

## III Conclusions

The passage sizes calculated above should give an expansion which draws equal air volume through all internal parts with a variation of less than .3% between maximum and minimum single part flow rate.

# AEROSOL LOSSES DURING PASSAGE THROUGH THE CHAMBER INLET SYSTEM (1-8)

D. J. Schleuter - D. R. White

The purpose of this study is to determine the fraction of aerosol particles lost during introduction of the sample into the chamber sensitive volume. The inlet system consists of the lowest expansion manifold with the top expansion manifold serving as the outlet. The flow is assumed to be laminar based on the Reynolds number. Volumetric flows of 3 liter/sec and 10 liter/sec were studied as the two extremes. The expansion manifold is broken up into four sections located symmetrically around the chamber and each of these has symmetry about the central inlet, therefore only one side of one section need be treated.

The flow velocity in each section of the manifold was first determined based on one-eighth of the total flow entering and being divided equally among the eighteen internal parts. The flow velocity given by

$$v = Q/(\pi r^2)$$

where Q is the volumetric flow rate and r the tube diameter, was used at each point to calculate the Reynolds number

$$Re = {}^{vd}/_{\nu}$$

to verify the laminar flow assumption. d is the passage diameter and $\nu$ is the kinematic viscosity.

Each individual section of passage within the manifold was then considered individually and the constant $\mu$, given by

$$\mu = {}^{Dx}/_{r^2\bar{v}}$$

where x is the passage length, r the radius, $\bar{v}$ is the mean fluid or aerosol velocity and assumed to equal the flow velocity calculated above. The diffusion coefficient D was taken from Fuchs (Mechanics of Aerosols, Pergamon Press, New York, 1964, p 184) for particles with radii of 1.0, 0.1, 0.01 and 0.001 micron.

Using the appropriate value of $\mu$ the fraction of particles of a given size passing through that section of manifold passage was determined from the expression

$${}^{\bar{n}}/_{r_o} = 1 - 2.56\mu^{2/3} + 1.2\mu + 0.177\mu^{4/3}$$

(Fuchs, p 205, Eq 39.3). The fractional concentrations of each section between the inlet and a particular interior port were then multiplied together to give a total effect. The results are listed in Tables 1 and 2.

Table 1 is for a total flow of 3 liter/sec while Table 2 is for 10 liters/sec. Each table is arranged in a 6 x 3 array of major divisions representing the eighteen interior ports. Column A is the ports closest to the inlet and column F those furthest from the inlet.

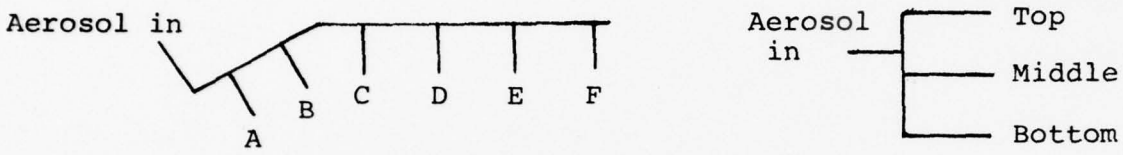


The three rows refer to the three levels of ports covered by one manifold. The results for each of the four particle sizes are given within each major division.

| ticle dius | A | B | C | D | E | F | |
|---|---|---|---|---|---|---|---|
| 0 | .4828 | .4632 | .4302 | .4293 | .4154 | .3687 | TOP |
| 1 | .9665 | .9649 | .9614 | .9613 | .9598 | .9562 | |
| 01 | .9977 | .9976 | .9974 | .9973 | .9972 | .9970 | |
| 001 | .9996 | .9996 | .9996 | .9996 | .9996 | .9995 | |
| 0 | .5429 | .5210 | .4837 | .4828 | .4671 | .4333 | MIDDLE |
| 1 | .9714 | .9690 | .9661 | .9661 | .9646 | .9610 | |
| 01 | .9980 | .9979 | .9977 | .9976 | .9975 | .9973 | |
| 001 | .9998 | .9997 | .9996 | .9996 | .9996 | .9996 | |
| 0 | .3538 | .3394 | .3151 | .3146 | .3044 | .2823 | BOTTOM |
| 1 | .9523 | .9505 | .9471 | .9470 | .9455 | .9420 | |
| 01 | .9966 | .9966 | .9964 | .9962 | .9962 | .9960 | |
| 001 | .9996 | .9995 | .9994 | .9995 | .9995 | .9994 | |

TABLE 1

Fractional concentration of aerosol entering chamber

Flow rate 3 liters/sec

| ticle ius | A | B | C | D | E | F | |
|---|---|---|---|---|---|---|---|
| 0 | .72812 | .71475 | .69118 | .69044 | .68020 | .65750 | TOP |
| 1 | .98483 | .98395 | .98236 | .98232 | .98160 | .98001 | |
| 01 | .99893 | .99892 | .99881 | .99880 | .99876 | .99865 | |
| 001 | .99985 | .99984 | .99982 | .99982 | .99981 | .99979 | |
| 0 | .76339 | .74938 | .72466 | .72389 | .71316 | .68936 | MIDDLE |
| 1 | .98704 | .98615 | .98455 | .98450 | .98379 | .98219 | |
| 01 | .99913 | .99637 | .99626 | .99895 | .99891 | .99610 | |
| 001 | .99987 | .99986 | .99984 | .99984 | .99983 | .99981 | |
| 0 | .63361 | .62198 | .60149 | .60083 | .59191 | .57216 | BOTTOM |
| .1 | .97819 | .97732 | .97573 | .97569 | .97497 | .97339 | |
| .01 | .99852 | .99846 | .99835 | .99834 | .99830 | .99819 | |
| .001 | .99978 | .99977 | .99975 | .99975 | .99974 | .99972 | |

TABLE 2

Fractional concentration of aerosol entering chamber

Flow rate 10 liters/sec

# APPENDIX D

## "A DIGITAL CONTROL PROGRAM FOR AN EXPANSION CLOUD CHAMBER"

K. Menke and D. E. Hagen

Presented at the meeting of the Missouri Academy
of Science, St. Louis, April, 1977

The following is the outline of a paper presented at the meeting of the Missouri Academy of Science describing the computer program developed to control the optical systems used to sense the cloud formation and development within the chamber. The program has been tested using an attenuation system operating in the visible red (.63μ) which permits the use of the attenuation system while the Mie scattering of blue green light (.488μ) and flash photographs of the cloud are also being acquired. The program can also take the data required to obtain at drop size spectrum of the cloud based on the Doppler frequency shift of scattered laser light.

This program or a modification will be required to control data acquisition during IR measurements in the large simulation chamber.

# A Digital Control Program for an Expansion Cloud Chamber

Kevin Menke and Donald Hagen

The Missouri Academy of Science Meeting, St. Louis, April, 1977

The purpose of this paper is to describe the methods used in a real time control and data acquisition program for a Cloud Simulation Chamber experiment.

The outline of the paper on slide one shows that first the elementary operation of the chamber will be discussed. The purpose of the program is to test several optical observation systems. Secondly these systems will be discussed. The third part of the paper shows the techniques used in the program.

The cloud simulation chamber may be thought of as a sealed metal canister. The canister is first filled with moist aerosol laden air. The contents are expanded, condensing the moisture on the aerosol.

Slide two shows the simulation chamber controlled by the Nova 840 minicomputer. The acquisitioning and control are those which are used in the program.

Slide three is a photograph of the Nova 840 and its peripherals. For this experiment data acquisition was done through a High Level Analog to Digital convertor as well as a Wide Range Analog to Digital convertor. Control is achieved through digital output.

The purpose of the program is to test four optical systems. These systems are shown in slide 4. They are:

1.) Attenuation - The light source is a light emitting diode. The information obtained is the clouds drop density and size.
2.) Doppler Shift - The light source is an argon-ion laser. The method informs one of the cloud's drop size spectrum.
3.) Mie Scattering - The light is supplied by the argon-ion laser. The information obtained is the drop size. The cloud must be monodisperse.
4.) Photography - One is able to count the drop density of the cloud.

Slide five shows the main parts of the multi-task fortran program called OPTTST (Optical Test). The program begins with the pre-expansion phase. The expansion initiates the tasks CAMERA, UCLOSE and STTORLD and follows with the post-expansion chores.

The time line of OPTTST (slide six) shows that during pre-expansion, time intervals for the expansion are accepted. The calculation constants needed in calculations during the post-expansion are read in. An initial set of data is recorded.

With the opening of the valve, task UCLOSE is initiated. It waits until time T1 has elapsed and then closes the expansion valve. Task CAMERA is also initiated. It waits until time T3 and begins taking

photographs. At each photo time task CAMERA is given control and the task closes the photomultiplier tube so that no damage is done to the measurement equipment due to the flash. The P-M tube is then opened after the picture has been taken. The task is done after a given number of photos have been taken. During the suspension of these tasks the program control is given to a main DO loop which reads data into data vectors and also signals the light beam oscillograph that data has been taken. Task STTORLD is initiated on the first loop to store doppler laser data on a binary file for future use.

The data loop will finish after 21 iterations (a time of T2 has elapsed). The post-expansion phase of the program calculates the pressure ratios and attenuation ratios. The results are immediately displayed on the CRT. One may also obtain a printout of the results of the expansion.

Some conclusions are that OPTTST shows that real time experiment programming is greatly simplified when one uses multi-tasking as a programming tool. One might as well point out that digital controlled experiments have great versatility as compared to analog controlled experiments. A wide variety of different experiments may be run by simply writing new soft ware.

# PAPER OUTLINE

1. CLOUD SIMULATION CHAMBER

2. TEST OPTICAL OBERVATION SYSTEMS

3. COMPUTER PROGRAM

# OPTTST

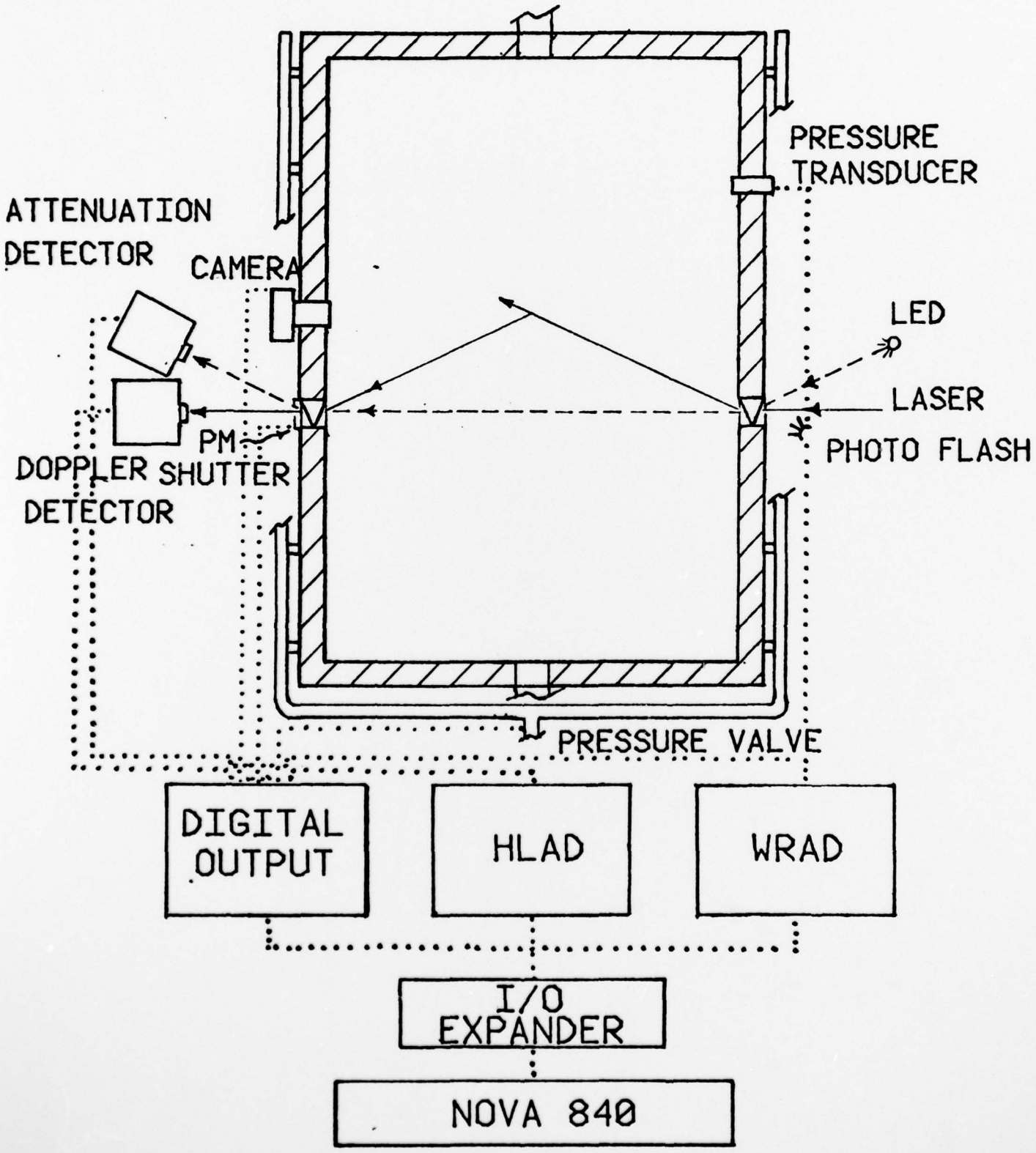
PRESSURE
TRANSDUCER
ATTENUATION
DETECTOR
CAMERA
LED
LASER
PM
SHUTTER
PHOTO FLASH
DOPPLER
DETECTOR
PRESSURE VALVE
DIGITAL
OUTPUT
HLAD
WRAD
I/O
EXPANDER
NOVA 840

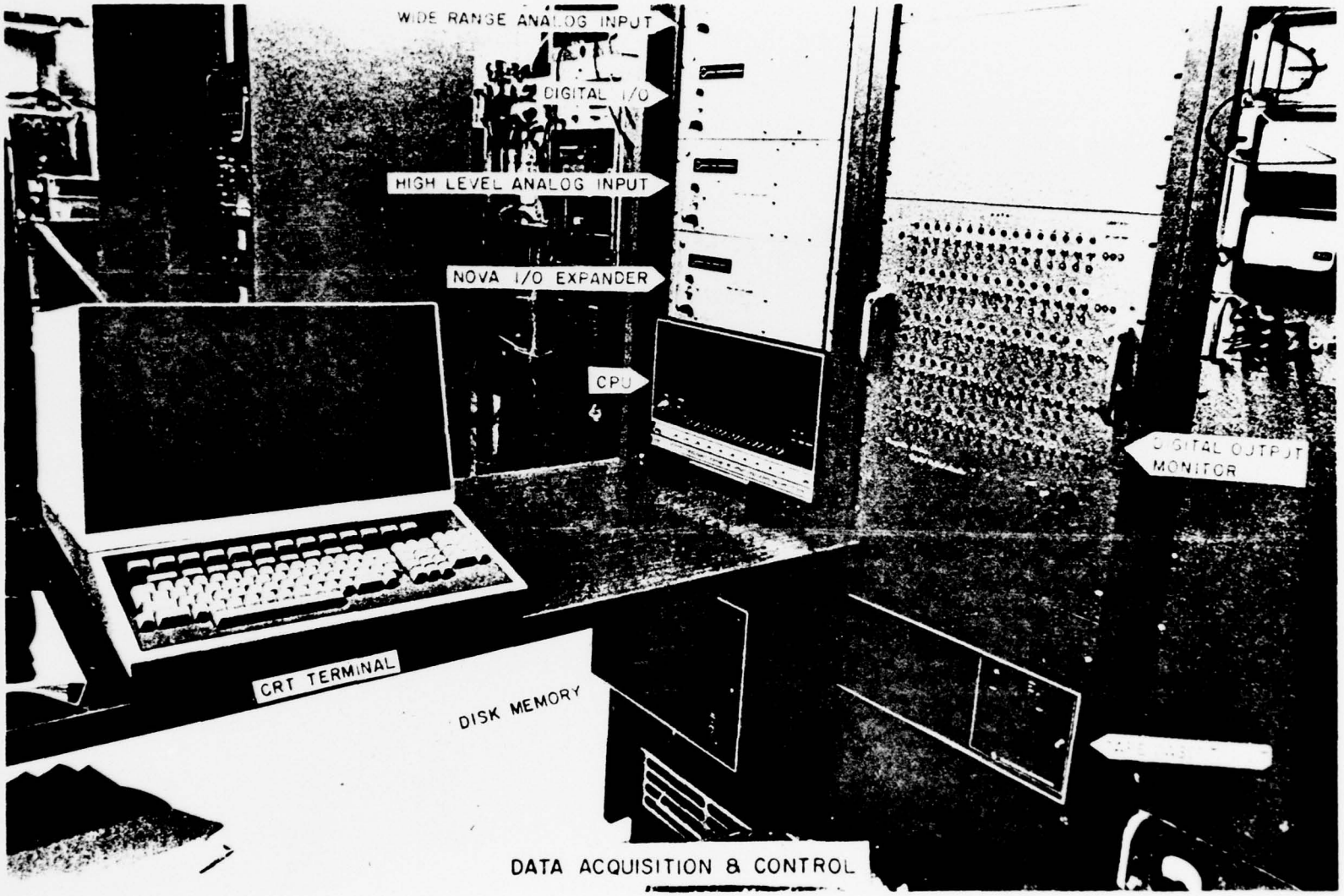


DATA ACQUISITION & CONTROL

# AVAILABLE OPTICAL OBSERVATION METHODS

1. ATTENUATION
    A. LED
    B. DROP DENSITY / SIZE

2. DOPPLER SHIFT
    A. ARGON-ION LASER
    B. DROP SIZE SPECTRUM

3. MIE SCATTERING
    A. ARGON-ION LASER
    B. DROP SIZE - MONODISPERSE CLOUD

4. PHOTOGRAPHY
    A. FLASH LAMP
    B. DROP DENSITY

# OPTTST FLOWCHART

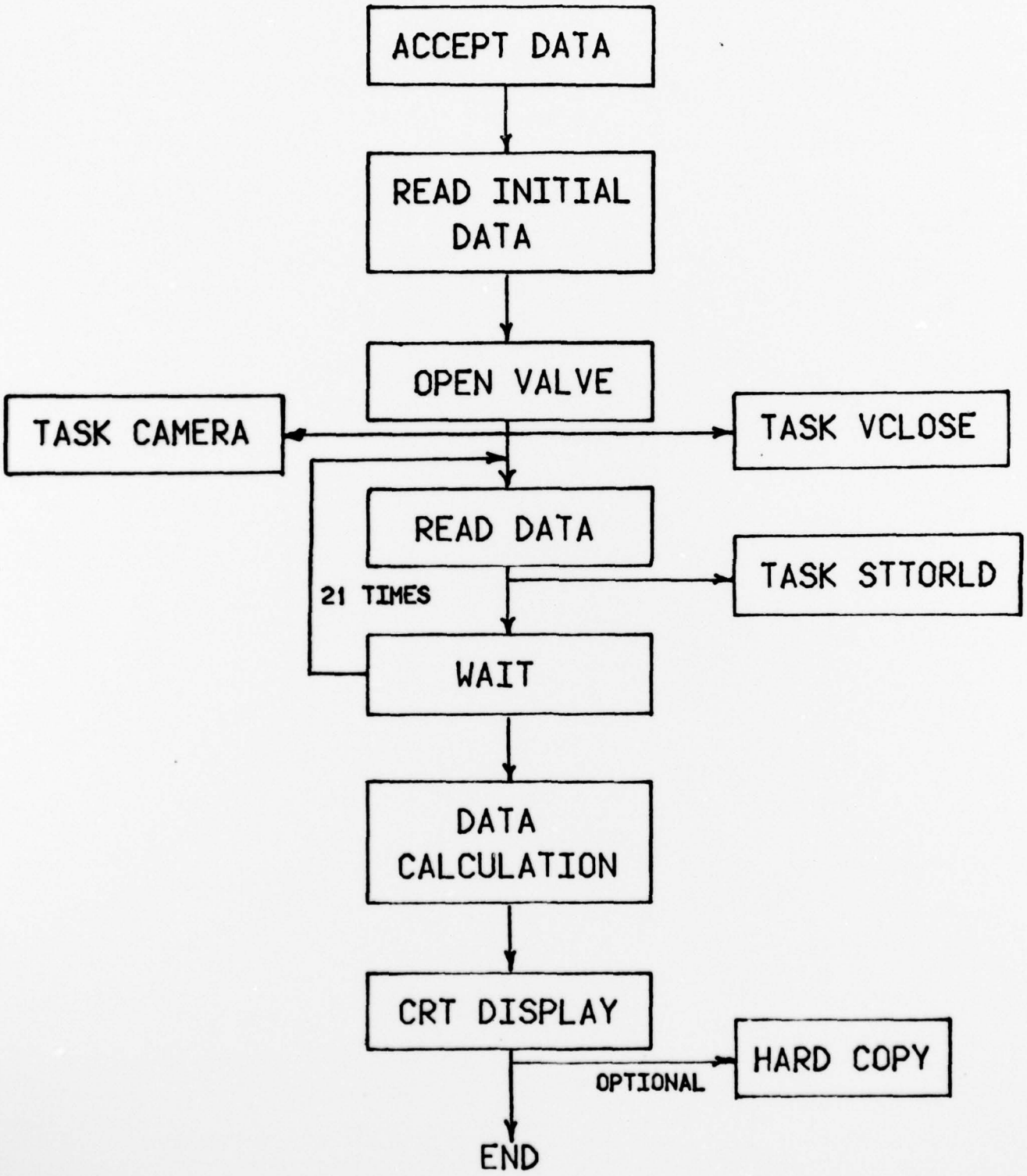

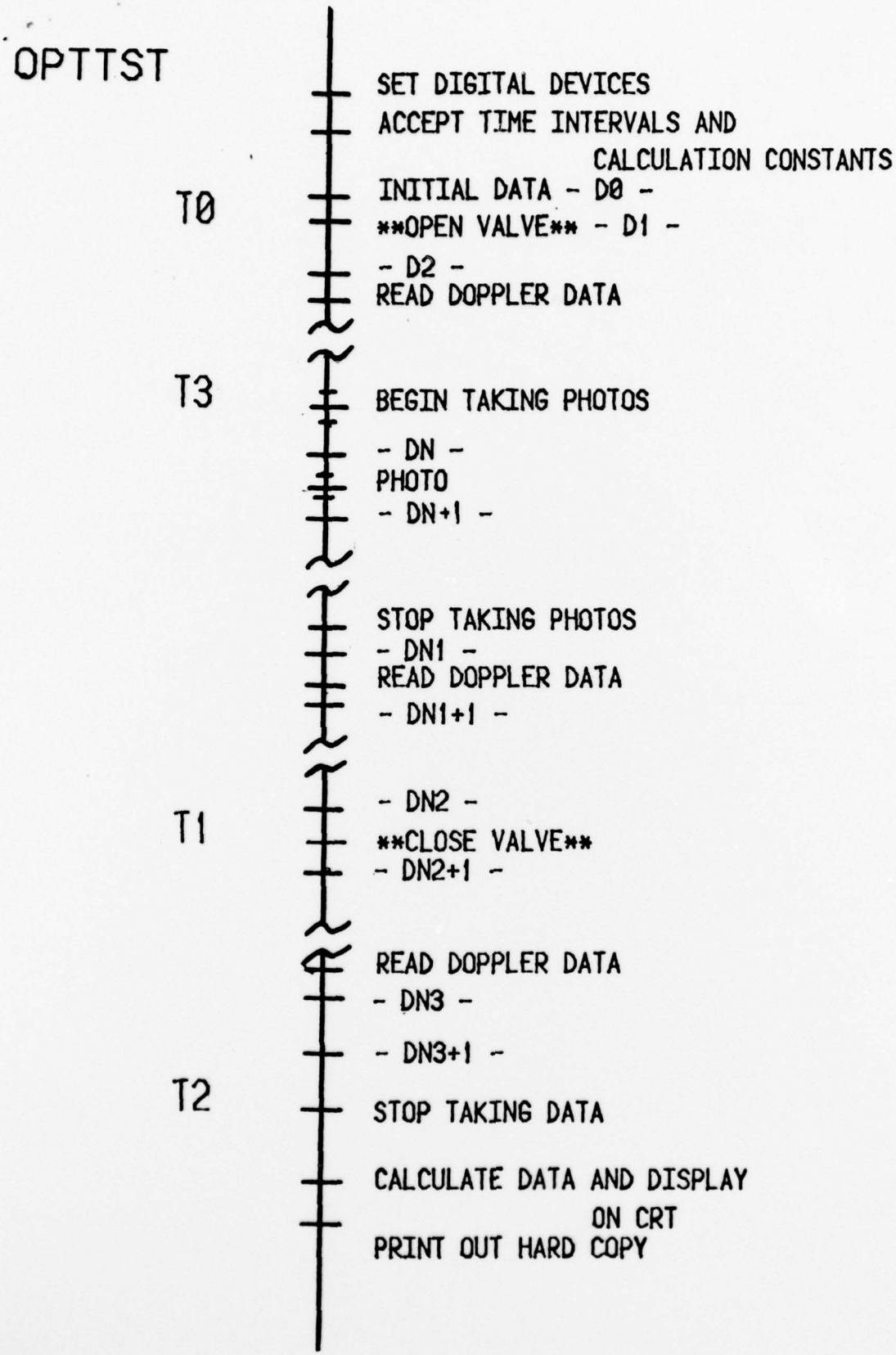
OPTTST
SET DIGITAL DEVICES
ACCEPT TIME INTERVALS AND
CALCULATION CONSTANTS
T0
INITIAL DATA - D0 -
**OPEN VALVE** - D1 -
- D2 -
READ DOPPLER DATA
T3
BEGIN TAKING PHOTOS
- DN -
PHOTO
- DN+1 -
STOP TAKING PHOTOS
- DN1 -
READ DOPPLER DATA
- DN1+1 -
- DN2 -
T1
**CLOSE VALVE**
- DN2+1 -
READ DOPPLER DATA
- DN3 -
- DN3+1 -
T2
STOP TAKING DATA
CALCULATE DATA AND DISPLAY
ON CRT
PRINT OUT HARD COPY

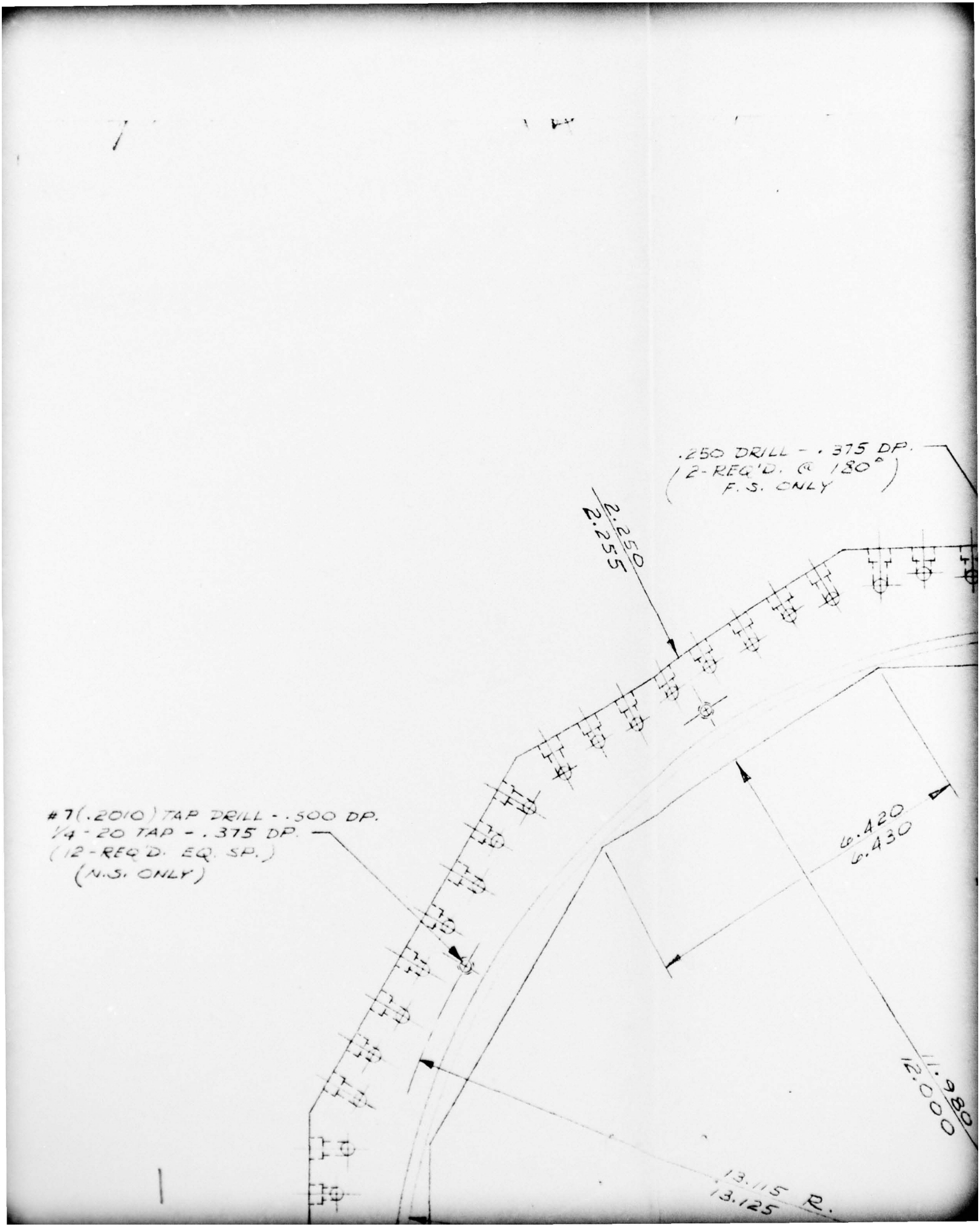
.250 DRILL - .375 DP.
(2-REQ'D. @ 180°
F.S. ONLY)
2.250
2.255
#7(.2010) TAP DRILL - .500 DP.
1/4 - 20 TAP - .375 DP.
(12-REQ'D. EQ. SP.)
(N.S. ONLY)
6.420
6.430
11.980
12.000
13.115 R.
13.125

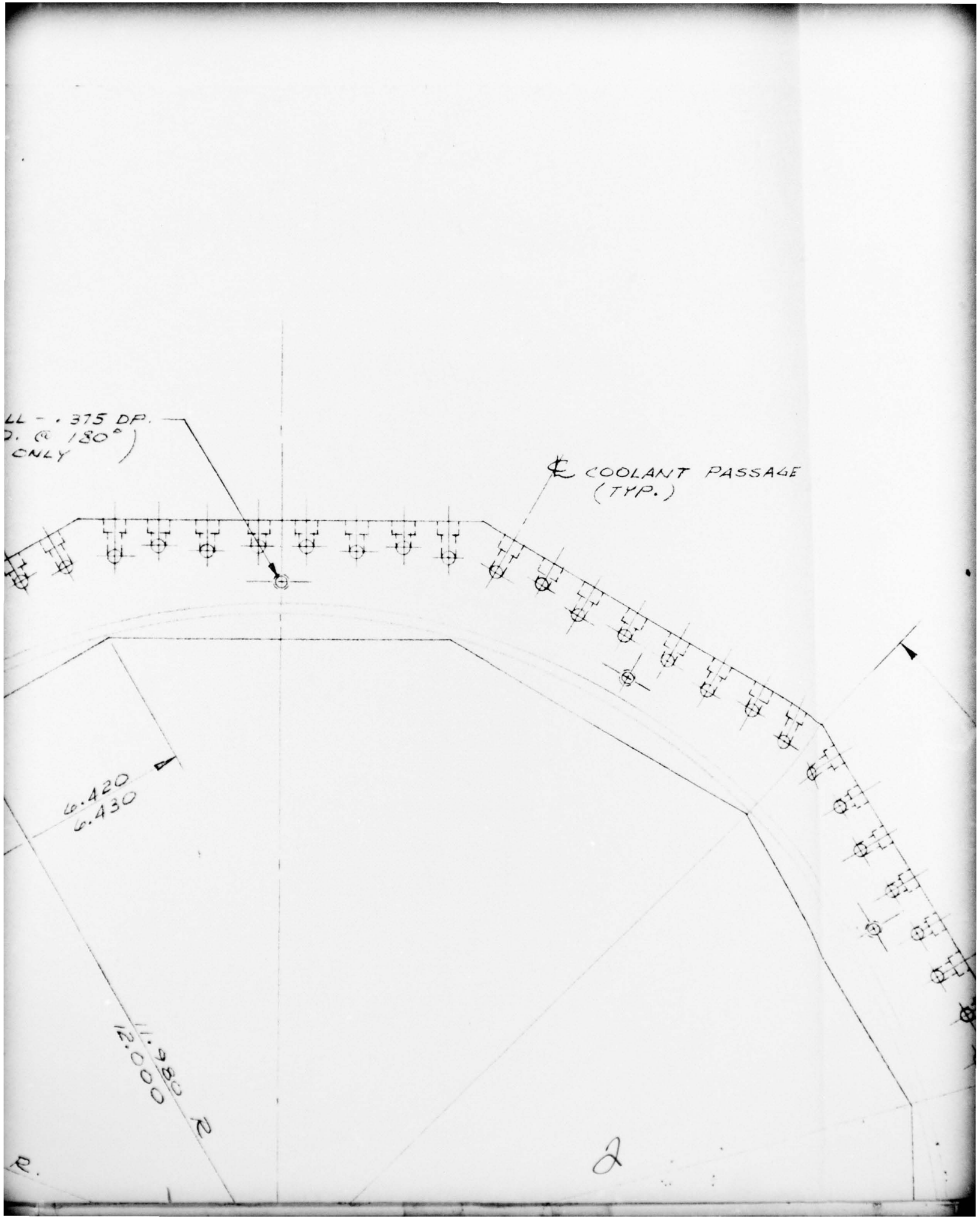
LL - .375 DP.
D. @ 180°
ONLY )
℄ COOLANT PASSAGE
(TYP.)
6.420
6.430
12.000
11.980
R.
2

PASSAGE

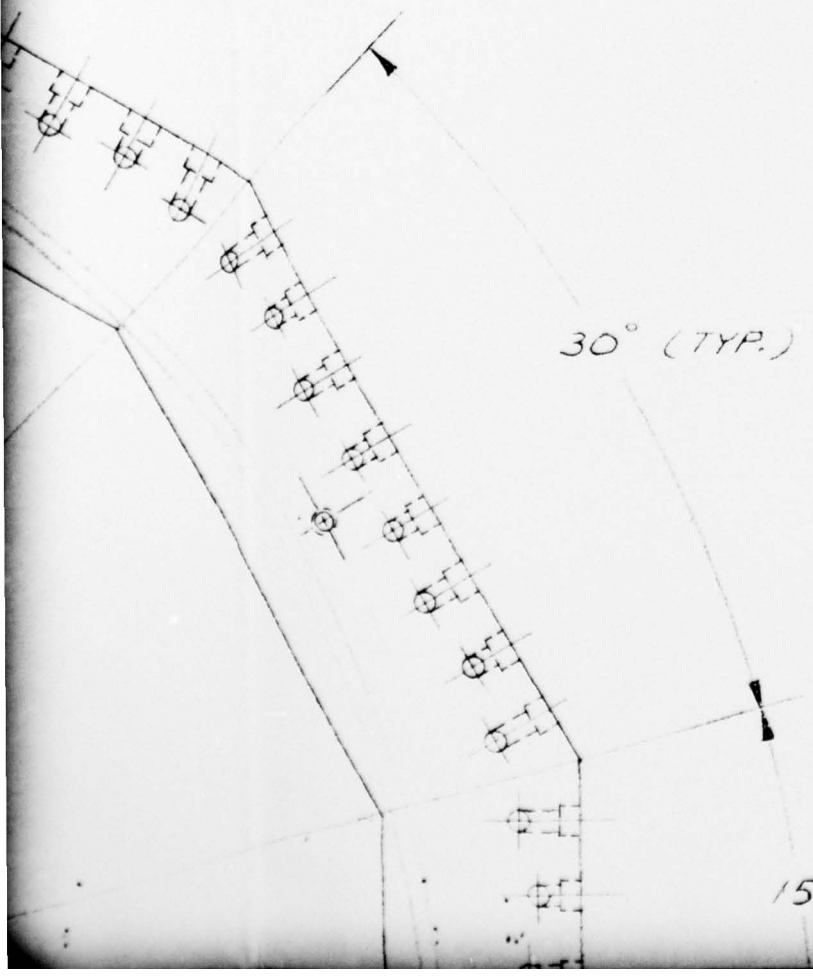

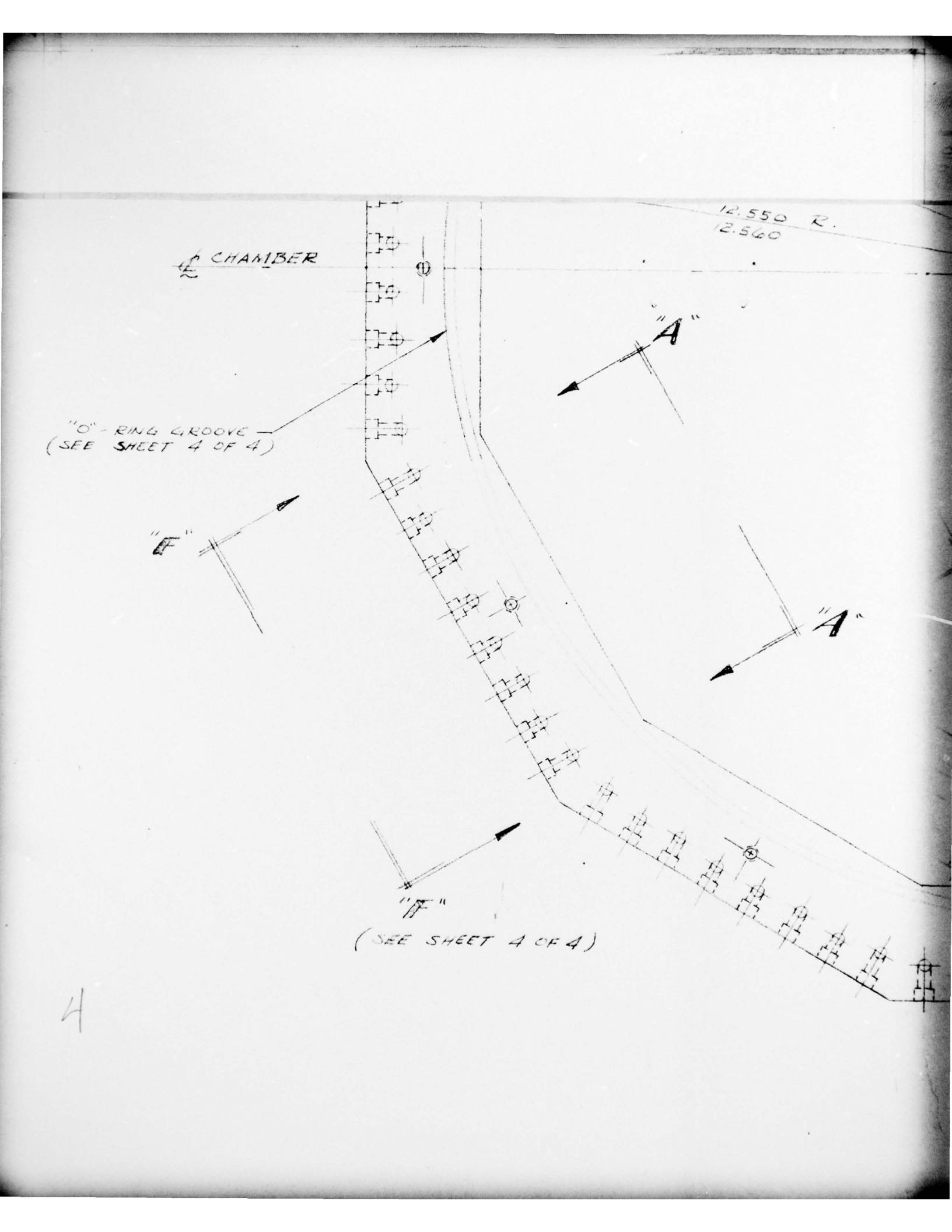
12.550 R.
12.560
℄ CHAMBER
"A"
"O" - RING GROOVE
(SEE SHEET 4 OF 4)
"F"
"A"
"F"
(SEE SHEET 4 OF 4)

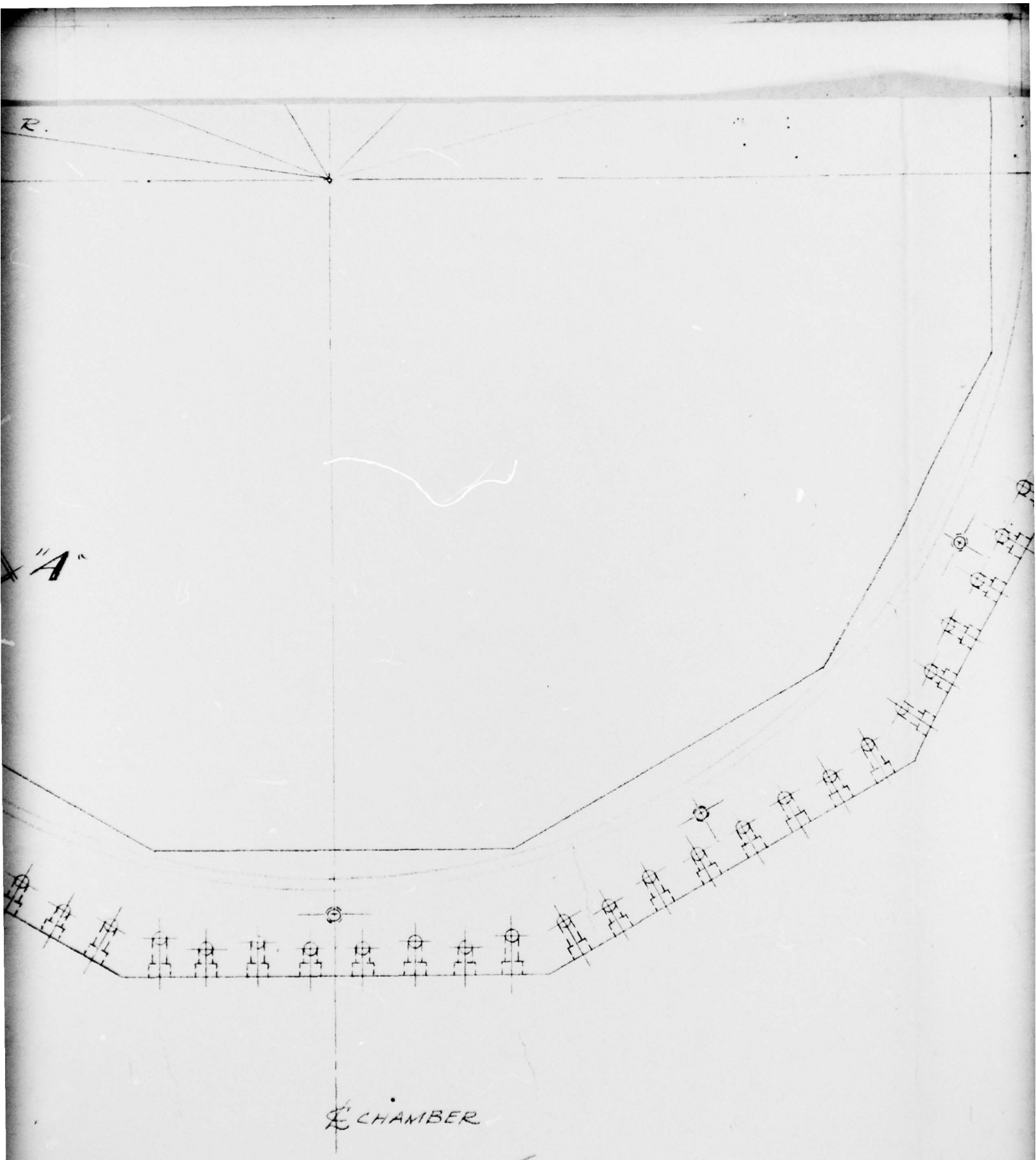


5

PLAN VIEW

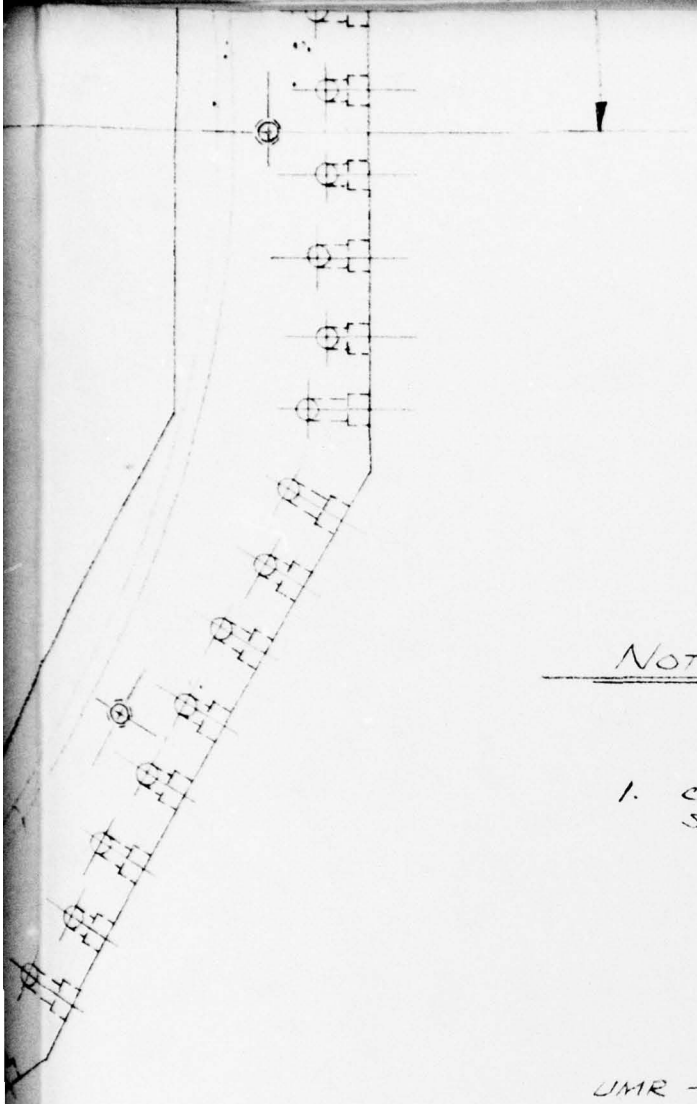

NOTE

1. COOLANT PASSAGES ARE SHOWN ONLY FOR CLARITY.

UMR - GCCPR SIMULATION PROJECT
CHAMBER SECTION ( HEAT SINK )
ALUMINUM
SCALE : 1/2" = 1"
1/6/77
TOM SCHASTEEN, JR.

6

SHEET 1 OF 11